Nanoscale Advances

ROYAL SOCIETY OF CHEMISTRY

PAPER

View Article Online
View Journal | View Issue

Cite this: *Nanoscale Adv.*, 2024, **6**, 3566

Triboelectric–electromagnetic hybrid nanogenerator for harvesting blue energy and creating an ocean wave warning system†

Weichao Wang, [a] Yaju Zhang,*[b] Guoxi Wu,[a] Zhengyin Zhao,[a] Yonghui Wu[b] and Haiwu Zheng[b]

The abundant water wave energy on Earth stands as one of the most promising renewable blue energy sources, as it exhibits minimal dependence on weather, time and temperature. However, the low fluctuation frequency and extremely irregular nature of the wave energy restrict both the methods and efficiency of energy harvesting. In this study, a packed box-like hybrid nanogenerator was designed, comprising two single-electrode triboelectric nanogenerators (TENGs) and two electromagnetic generators (EMGs). The outputs of both the TENG and EMG were demonstrated under different fluctuation frequencies and swing amplitudes, inspiring the development of a wave warning system. The maximum output voltage, current, and transferred charge of the single TENG, as part of hybrid nanogenerator (HG), reach approximately 110 V, 2.3 μA, and 50 nC, respectively. Its peak power reaches 85.3 μW under a resistance load of 20 MΩ at a frequency of 2 Hz. The EMG component produced maximum output voltages and currents of up to 0.45 V and 1.2 mA, respectively. The peak power is approximately 95.6 μW with a resistance load of 200 Ω. The output performances of the TENG and EMG increase linearly with the increase in the swing angle. Most importantly, a packed box-like hybrid nanogenerator can be conveniently packaged for harvesting energy from water waves. A wave energy collection array floating on the sea is proposed for harvesting blue energy and creating a self-powered ocean wave warning system.

Received 17th March 2024
Accepted 6th May 2024

DOI: 10.1039/d4na00222a

rsc.li/nanoscale-advances

Introduction

Human society relies heavily on fossil fuels such as coal, oil and natural gas to meet its energy needs. However, the use of these fuels results in carbon emissions that contribute to today's climate problems, such as air pollution and acid rain.[1,2] In response to the policies on carbon peaking and neutrality, human beings need to search for renewable, clean energy sources, such as solar energy, wind energy, and ocean energy, for sustainable development.[3,4] Among renewable energy sources, ocean energy, which covers 70% of the Earth's surface remains largely underexploited, and it is not strongly dependent on weather, time or temperature. Traditional electromagnetic generators for harvesting ocean energy are costly, cumbersome and inefficient, particularly under low frequencies. Based on the coupling of the triboelectric effect and electrostatic induction, triboelectric nanogenerators (TENGs) offer a feasible pathway for achieving higher energy harvesting efficiency from low frequency mechanical energy, such as vibrations, human walking, body motions, and ocean waves.[5–9] Moreover, TENGs have the advantages of high output energy and conversion efficiency, ease of manufacture, low cost, flexibility, and abundant choice of materials.[10–18] The usage of a series of triboelectric nanogenerators has be extended to harvesting water wave energy and sensing, as well as electrostatic energy at the liquid–solid interface.[19–27]

A packaging strategy for TENGs is necessary to withstand the environmental changes. Wave warning systems play a notable role in marine exploration, fishery, maritime transportation, *etc.* However, current warning devices require substantial engineering investment, are costly, need long periods of construction, and consume significant manpower and material resources.[28–31] Therefore, to effectively harvest multidirectional and a broad frequency range of ocean energy, a self-powered wave warning system with advanced structural design and related applications needs to be developed.

In this work, a packed box-like HG is designed, consisting of two single-electrode TENGs and two EMGs. Owing to its superior structural design characteristics, both TENGs can operate simultaneously within a frequency cycle, while the EMGs can operate twice within a fluctuating cycle, effectively doubling the

[a]*School of Science, Xuchang University, Xuchang 461000, China*
[b]*International Joint Research Laboratory of New Energy Materials and Devices of Henan Province, School of Physics and Electronics, Henan University, Kaifeng 475004, China. E-mail: 40070002@vip.henu.edu.cn*

† Electronic supplementary information (ESI) available. See DOI: https://doi.org/10.1039/d4na00222a

frequency. The output performances of the TENG and EMG are demonstrated under varying fluctuation frequencies and swing amplitudes. The maximum output voltage, current, and charge transfer amount of the single TENG is approximately 110 V, 2.3 μA and 50 nC, respectively. Its peak power is 85.3 μW under the resistance load of 20 MΩ at a frequency of 2 Hz. The maximum output voltage and current of a single EMG are about 0.45 V and 1.2 mA, respectively. The peak power is about 95.6 μW at a resistance load of 200 Ω. Based on the characteristics of the HG, we propose a wave energy collection array floating on the sea surface for blue energy harvesting and wave warning purposes.

Experimental section

Fabrication of the box-HG

The cuboid poly(methyl methacrylate) (PMMA) box-HG was composed of TENG and EMG components. A laser cutter was employed to cut 3 mm thick PMMA sheets into rectangular shapes with various dimensions to serve as the walls of the cuboid box. For the preparation of TENG, a PMMA sheet (105 mm × 50 mm × 3 mm) was used as the bottom supporting substrate, with two additional PMMA sheets each 2 mm thick, attached as arc-shaped tracks on both sides, positioned 6 mm above the bottom PMMA.

In the next step, two copper foils (100 mm × 80 mm × 0.065 mm) were adhered to two PMMA plates (120 mm × 105 mm × 3 mm), respectively. These plates were securely fixed to the two long edges of the bottom PMMA supporting plate. Following that, two rectangular holes (length: 80 mm, width: 3 mm) were created in the middle of the PMMA, matching the size of the bottom support plate, to secure the PTFE film as a triboelectric layer. The PTFE surface with nanostructures was fabricated using inductively coupled plasma (ICP) etching.[32] Two copper wires were drawn from the two copper foils to serve as the two electrodes of the TENG. Then, two PMMA plates (125 mm × 54 mm × 3 mm) were fixed onto the rectangular box as the side support plates. For the fabrication of EMG, a magnetic bar was passed through the lower part of the PTFE to slide freely within the two arc-shaped tracks. At the corresponding position to the magnetic bar, the two copper coils were fixed in the middle of the bottom side of the PMMA plate. The two terminals of the copper coil were used as the electrodes of the EMG. Finally, all the parts were pasted and sealed using hot glue.

Electrical measurement of the HG

The open-circuit voltage (V_{oc}), short-circuit current (I_{sc}), and short-circuit transferred charge (Q_{sc}) of the devices were measured by using a Keithley 6514 system electrometer. The HG was driven using a linear motor, and its output performance was measured at various operational frequencies. The measurement software platform was developed using LabVIEW, which is capable of real-time data acquisition and analysis applications. The surface morphology of the PTFE film, functioning as a triboelectric layer, was characterized using field emission scanning electron microscopy (SEM, JSM-7001F).

Results and discussion

Structural design and working principle

Fig. 1a and c show the schematic diagram and photograph of the HG, respectively. The PTFE surface with nanostructures depicted in Fig. 1b can improve the surface charge density of contact electrification by increasing the surface area between the bent nanostructures of PTFE and the Cu electrode. Fig. 2 illustrates the electricity generation process mechanism of the TENG and EMG nanogenerators, respectively, including the production of short-circuit current, and charge distribution for the TENG (Fig. 2a) and magnetic flux for the EMG (Fig. 2b). As evident from Fig. 2a(i), when the device is stationary, there is no electron transfer between the copper electrode and the grounding terminal. Meanwhile, the magnetic flux in the copper coils does not change as the magnetic bar is in the middle of the bottom track, as shown in Fig. 2b(i); thus no short-circuit current is generated. When the device swings left under the action of waves, a positive potential is generated during the closing of the PTFE film to contact the copper electrode, and electrons flow from the Cu electrode to the ground due to the coupling of surface potential difference and the electrostatic induction effect, as shown in Fig. 2a(ii). At this time, the magnetic flux crossing the copper coil will abate, resulting in an inductive electromotive force produced in the copper coils (Fig. 2b(ii)). When the device oscillates to the maximum angle (Fig. 2a(iii)), electron transfer does not occur in the circuit because an electrostatic balance is reached between the two materials, PTFE film and the copper electrode. For EMG, the unchanged magnetic flux does not induce short-circuit current generated in the coil, as shown in Fig. 2b(iii). When the device recovers from the maximum swing angle, the PTFE film is separated from the right copper electrode, as shown in Fig. 2a(iv). Electrons flow from the ground to the right copper electrode, resulting in an opposite current signal. As the device returns to the initial position, no electric signal is generated. The aforementioned process constitutes half of a swing cycle. As it continues to swing to the right, contact-separation process between PTFE and the left electrode will produce a triboelectric potential. Simultaneously, as the magnetic rod moves to the left, the change in magnetic flux in the copper coils induces the generation of a current signal.

Output performance of the HG

To characterize the performance of harvesting wave energy, the output performance of both the TENG and EMG were measured and analyzed using a programmable linear motor. Fig. 3a–d provide a clear quantitative comparison of the electrical outputs of the TENG at different operation frequencies and oscillation angle of 60 degrees. As the operation frequencies increase from 0.5 to 2.0 Hz, the maximum values of V_{oc}, I_{sc} and Q_{sc} increase from about 88 V, 0.88 μA and 35 nC to about 110 V, 2.4 μA and 45 nC, respectively, as shown in Fig. 3a–c. It is evident that the electrical output signal increases approximately linearly with the increase in operating frequency (Fig. 3d). It is well known that the magnitude of open circuit voltage and

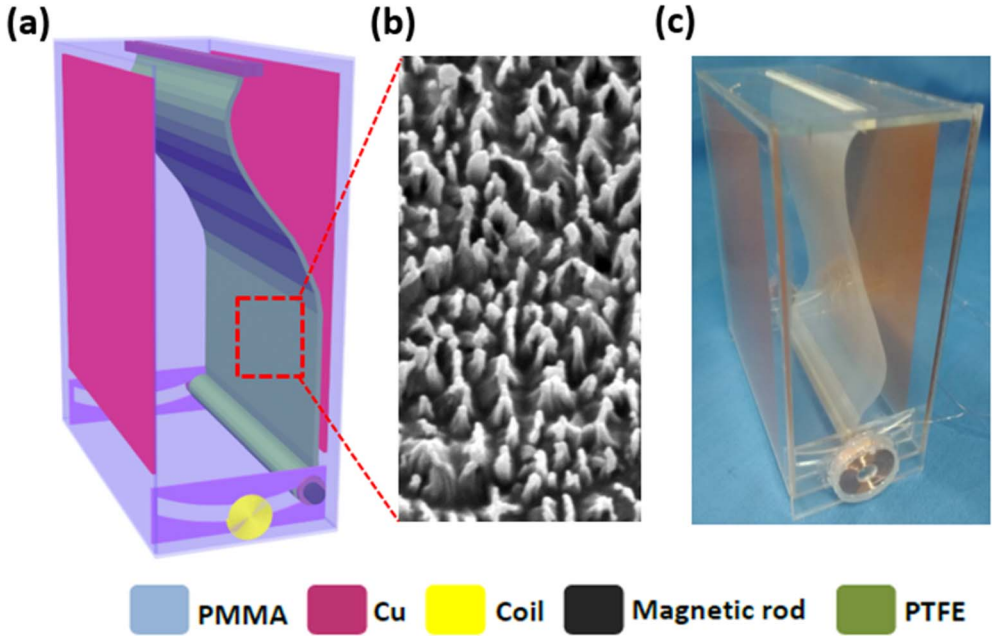

Fig. 1 (a) The schematic diagram of structural design and (b) the SEM images of the PTFE surface showing nanostructures. (c) Photograph of the HG.

transferred charge are related to their contact area.[33–35] Given that the oscillation speed increases as the working frequency increases in HG, the improved impulse of the PTFE provides a greater impact force. This results in the increased contact force between PTFE and copper electrode. The transfer rate of the output charge determines the magnitude of short-circuit current. This is because that a higher swing frequency will result in a larger output charge within a shorter time. Fig. 3e depicts the dependence of the output performance of TENG on various load resistances at an operating frequency of 2 Hz and an oscillation angle of 60 degrees. The voltage increases gradually with load, while the current shows an opposite trend. The

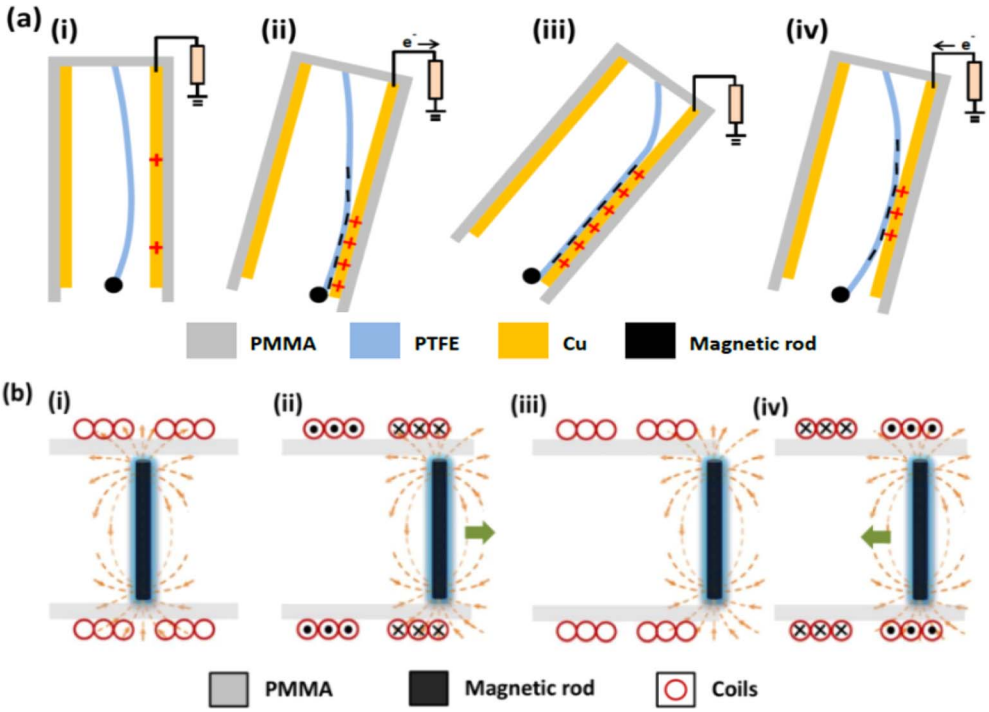

Fig. 2 The mechanism for the electricity generation process of TENG (a) and EMG (b) in HG.

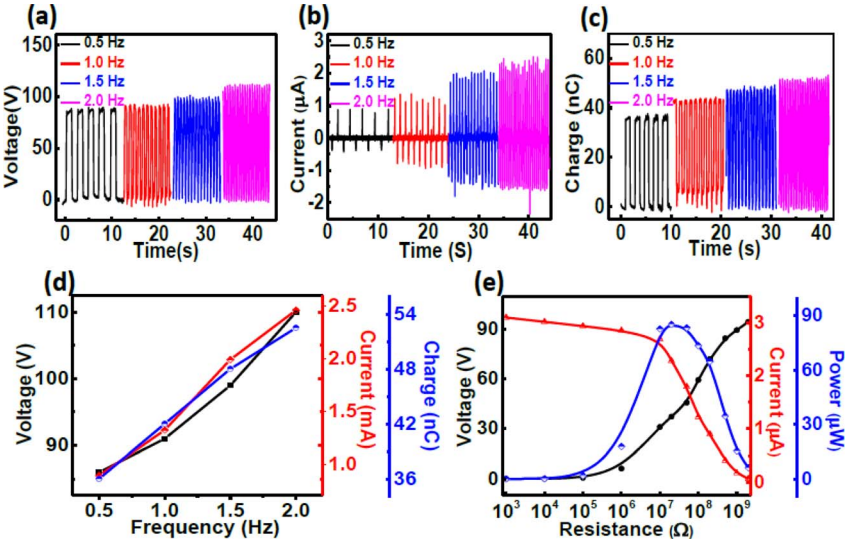

Fig. 3 (a)–(c) The V_{oc}, I_{sc} and Q_{sc} of the TENG at different operation frequencies and 60 degree of oscillation angle in HG, respectively. (d) The dependence of the V_{oc}, I_{sc} and Q_{sc} of the TENG on operation frequencies. (e) Output performances of the TENG at the frequency of 2 Hz and different external resistance loads.

largest instantaneous peak power of the TENG is about 85.3 μW at a loading resistance of 20 MΩ. Fig. 4 displays the output performance of the EMG under different operation frequencies and an oscillation angle of 60 degrees. The V_{oc} of the EMG increases slowly with the frequency, and its value increases from ~0.39 V to ~0.44 V within the operating frequency range of 0.5–2 Hz (Fig. 4a). The I_{sc} of the EMG follows a similar trend to that of voltage, which increases from ~0.6 to ~1.22 mA (Fig. 4b). As shown in Fig. 4c, V_{oc} and I_{sc} have an approximate linear relationship with the increase of operating frequency. Based on the theory of electromagnetic induction, the magnitude of V_{oc} increases gradually when the change rate of the magnetic flux increases while the turns of the coil remain constant. The I_{sc} of the EMG increases with the increase in voltage, assuming that the resistivity of the coil is constant. Fig. 4d depicts the dependence of the output power, voltage and current signals on the external variable resistance (with a loading resistance range from 10 to 8000 Ω) at an operating frequency of 2 Hz. The output voltage for the EMG increases as the external resistance load increases, whereas the output current shows the opposite trend.

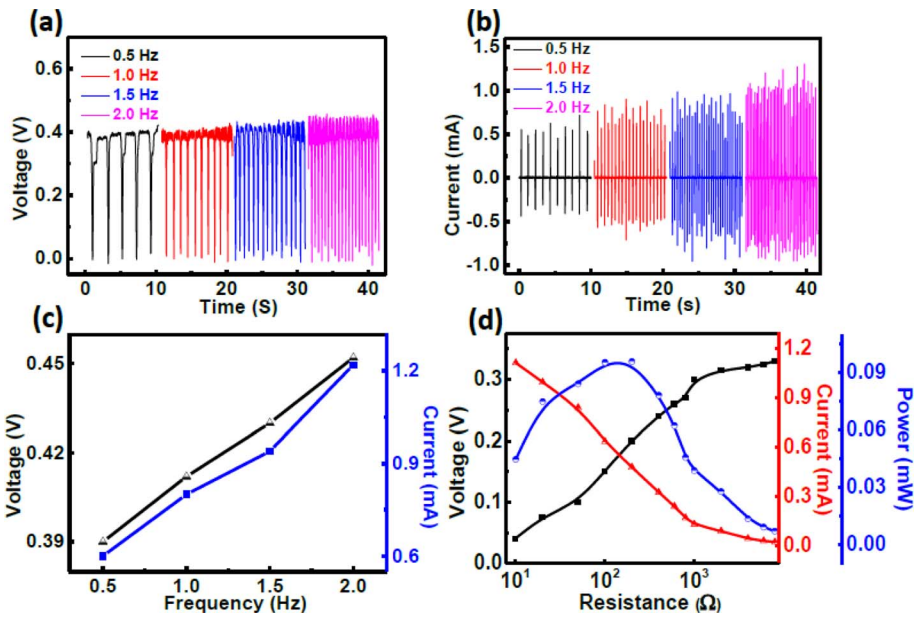

Fig. 4 (a) The V_{oc} and (b) I_{sc} of the EMG at different operation frequencies and 60 degree of oscillation angle in HG, respectively. (c) The dependence of the V_{oc} and I_{sc} of the EMG on operation frequencies. (d) Output performances of the EMG at the frequency of 2 Hz and different external resistance loads.

The largest instantaneous power is 95.6 μW at the external loading resistance of up to 200 Ω. The optimal external loading resistance for the EMG does not align with the value of 20 MΩ for the TENG. Usually, a circuit management unit or transformer is employed to address the impedance matching issue between the EMG and TENG in the practical application of HG.

The influence of oscillation angle on the output performance of TENG is systematically investigated at the operating frequency of 1 Hz, as depicted in Fig. 5. The V_{oc}, I_{sc} and Q_{sc} of the TENG increase from ~45 V to ~96 V, from ~0.25 μA to ~1.6 μA, and from ~18 nC to ~40 nC, respectively, as the oscillation angle increases from 15 to 90 degree (Fig. 5b–d).

In order to clearly understand the influence of the oscillation angle on the output performance of the TENG, we set up a simple pendulum model, as illustrated in Fig. 5a. The arc length of the swing can be calculated using the following equation:

$$L = \frac{\partial \pi r}{180} \tag{1}$$

where ∂ is the oscillation angle of the device, and m, f and r are the mass, operation frequencies, and swing radius of the device, respectively. The running time from the maximum angle to $\partial = 0$ is about $t = \frac{1}{4f}$. The running velocity of the device at $\partial = 0$ can be obtained from the following formula:

$$v = \frac{L}{t} = 4Lf \tag{2}$$

Merging eqn (1) and (2), we can obtain the running velocity of the device as

$$v = \frac{\partial \pi r/180}{1/4f} = \frac{\partial \pi r f}{45} \tag{3}$$

Since the given device mass is constant, its momentum can be expressed as

$$\Delta P = mv = \frac{m\partial \pi r f}{45} \tag{4}$$

Finally, when the device reaches the bottom, the force between PTFE and the copper electrode can be calculated using the following formula

$$F = \frac{\Delta P}{t} = \frac{m\partial \pi r f^2}{45} \tag{5}$$

According to eqn (3), the running speed of the EMG is proportional to the operating frequency. An increase in operating frequency enhances the electrical output performance of the EMG (Fig. 4). Moreover, the running speed of EMG is proportional to the swing angle at an exact operating frequency. The increased rate of change of the magnetic flux in the coils promotes the electrical output performance, as shown in Fig. 5b and c.

According to eqn (5), the force between the PTFE and the copper electrode is proportional to the square of the frequency and the oscillation angle. On the one hand, the increase of frequency is beneficial for improving the electrical output performance of the TENG at a specific swing angle, which is consistent with the measurement results in Fig. 3. On the other hand, the increased contact area of the friction layers from 15 to 90 degree contributes to boosting the electrical output performance of the TENG, as shown in Fig. 5d–f.

Applications

To effectively utilize the capability of the HG consisting of TENG and EMG as a sustainable power source, two full-wave bridge rectifiers connected in parallel were employed to charge

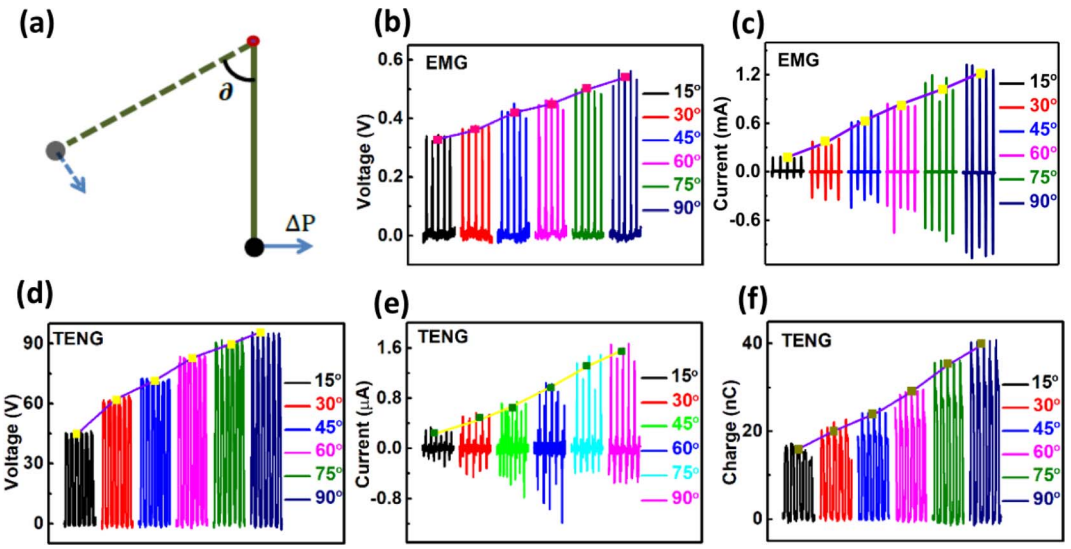

Fig. 5 (a) Oscillating model of HG. (b) The V_{oc} and (c) I_{sc} of the EMG at different oscillation angles and the operation frequency of 1 Hz in HG, respectively. (d) The V_{oc}, (e) I_{sc} and (f) Q_{sc} of the TENG at different oscillation angles and the operation frequency of 1 Hz in HG, respectively.

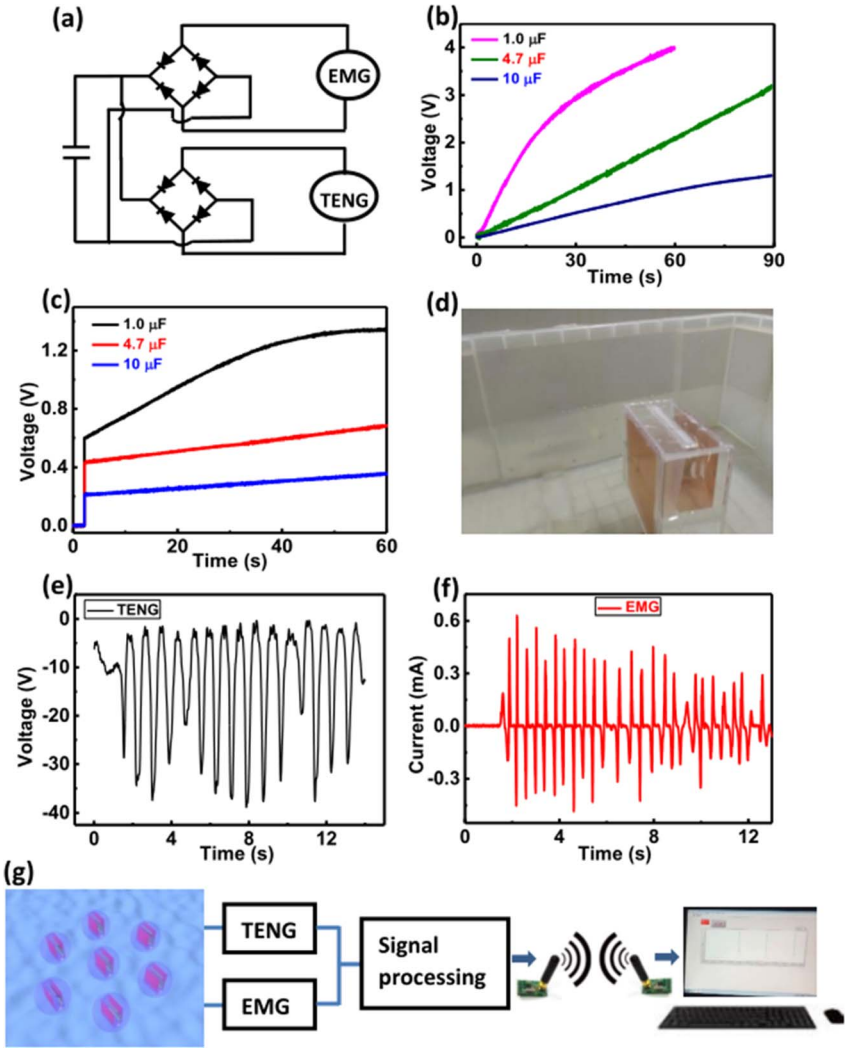

Fig. 6 Demonstration of the packaged HG as a practical power source. (a) The circuit diagram for charging capacitors. The charging curves of different capacitors using either (b) TENG or (c) EMG at the operation frequency of 1 Hz. (d) The photograph of HG in a water tank. (e) The fluctuation in V_{oc} of TENG and the (f) I_{sc} of the EMG in water wave. (g) Diagram of HG system for wave warning in the ocean.

different capacitors (1, 4.7, and 10 μF), as shown in Fig. 6a. Fig. 6b demonstrates that larger capacitors charged by the TENG at the frequency of 2 Hz require more charging time.[36,37] When the capacitor is charged by the EMG at the frequency of 2 Hz, the voltage is limited by the low open-circuit voltage of EMG and saturates in a short charging time,[38,39] as shown in Fig. 6c. To further scale HG for practical applications, the packaged device is placed in a water tank and fixed (Fig. 6d). As depicted in Fig. 6e and f both the output voltage of the TENG and the output current of the EMG exhibit fluctuation characteristics in water waves.

According to the output characteristics of the HG, and to further expand the practice application of HG, we propose that the HG arrays be utilized to harvest blue energy for acting as a self-powered ocean wave warning system to monitor the changes of ocean waves. The TENG and EMG produce the voltage and current outputs under ocean waves, which are then transmitted as electric signals to the terminals of the computer or the mobile phone. When the output voltage of the TENG and the output current of the EMG exceed specific set values generated by larger ocean waves, an alarm signal cautions that the ocean waves are too large at that time to venture into the sea. The simulated wave warning process of the HG in the water tank is shown in Videos S1 and S2.†

Conclusions

In summary, a packed box-like hybrid-nanogenerator consisting of two TENGs and two EMGs is designed for harvesting blue ocean energy. The output performances of TENG and EMG increase with an increase in the swing frequency and oscillation amplitude. For the TENG, a larger swing angle means a greater impulse, which improves the friction area of the TENG. For the EMG, the change rate of its magnetic flux increases with the increase in the swing angle. Based on the output characteristics of the HG, the designed HG has potential application in

harvesting blue energy, acting as a self-powered wave warning system to monitor the changes in ocean waves.

Conflicts of interest

There are no conflicts to declare.

Acknowledgements

This work was supported by the National Natural Science Foundation of China (No. 52072111), the Natural Science Foundation of Henan Province in China (No. 212300410004, 232300421211 and 222300420125), the Key Scientific Research Project of Colleges and Universities in Henan Province (23A140024), and the National Research Project Cultivation Foundation of Xuchang University (2023GJPY016).

Notes and references

1 C. G. Zhang, W. Yuan, B. F. Zhang, J. Y. Yang, Y. X. Hu, L. X. He, X. J. Zhao, X. H. Li, Z. L. Wang and J. Wang, *Small*, 2023, 2304412.
2 T. Jiang, L. M. Zhang, X. Chen, C. B. Han, W. Tang, C. Zhang, L. Xu and Z. L. Wang, *ACS Nano*, 2015, **9**, 12562.
3 T. Cheng, J. Shao and Z. L. Wang, *Nat. Rev. Methods Primers*, 2023, **3**, 39.
4 H. B. Lin, M. H. He, Q. S. Jing, W. F. Yang, S. T. Wang, Y. Liu, Y. L. Zhang, J. Li, N. Li, Y. W. Ma, L. H. Wang and Y. N. Xie, *Nano Energy*, 2019, **56**, 269.
5 Z. Wen, J. Chen, M.-H. Yeh, H. Guo, Z. Li, X. Fan, T. Zhang, L. Zhu and Z. L. Wang, *Nano Energy*, 2015, **16**, 38.
6 W. Ou-Yang, L. Q. Liu, M. J. Xie, S. Q. Zhou, X. W. Hu, H. Wu, Z. Y. Tian, X. C. Chen, Y. R. Zhu and J. Li, *Nano Energy*, 2024, **120**, 109151.
7 X. L. Wei, Z. H. Zhao, C. G. Zhang, W. Yuan, Z. Y. Wu, J. Wang and Z. L. Wang, *ACS Nano*, 2021, **15**, 13200.
8 H. Q. Gao, M. G. Hu, J. F. Ding, B. L. Xia, G. L. Yuan, H. S. Sun, Q. H. Xu, S. Y. Zhao, Y. W. Jiang, H. Wu, M. Yuan, J. H. Li, B. X. Li, J. Zhao, D. W. Rao and Y. N. Xie, *Adv. Funct. Mater.*, 2023, **33**, 2213410.
9 Y. Zou, Y. S. Gai, P. C. Tan, D. J. Jiang, X. C. Qu, J. T. Xue, H. Ouyang, B. J. Shi, L. L. Li, D. Luo, Y. L. Deng, Z. Li and Z. L. Wang, *Fundam. Res.*, 2022, **2**, 619.
10 Z. L. Wang, J. Chen and L. Lin, *Energy Environ. Sci.*, 2015, **8**, 2250.
11 Y. Zi, S. Niu, J. Wang, Z. Wen, W. Tang and Z. L. Wang, *Nat. Commun.*, 2015, **6**, 8376.
12 G. Zhu, J. Chen, T. Zhang, Q. Jing and Z. L. Wang, *Nat. Commun.*, 2014, **5**, 3426.
13 Z. Li, J. Chen, J. Zhou, L. Zheng, K. C. Pradel, X. Fan, H. Guo, Z. Wen, M.-H. Yeh, C. Yu and Z. L. Wang, *Nano Energy*, 2016, **22**, 548.
14 J. Chen, J. Yang, H. Guo, Z. Li, L. Zheng, Y. Su, Z. Wen, X. Fan and Z. L. Wang, *ACS Nano*, 2015, **9**, 12334.
15 C. Wu, X. Wang, L. Lin, H. Guo and Z. L. Wang, *ACS Nano*, 2016, **10**, 4652.
16 J. Wang, Z. Wen, Y. Zi, P. Zhou, J. Lin, H. Guo, Y. Xu and Z. L. Wang, *Adv. Funct. Mater.*, 2016, **26**, 1070.
17 G. Li, S. K. Fu, C. Y. Luo, P. Wang, Y. Du, Y. T. Tang, Z. Wang, W. C. He, W. L. Liu, H. Y. Guo, J. Chen and C. G. Hu, *Nano Energy*, 2022, **96**, 107068.
18 J. M. Liu, N. Y. Cui, T. Du, G. D. Li, S. H. Liu, Q. Xu, Z. Wang, L. Gu and Y. Qin, *Nanoscale Adv.*, 2020, **2**, 4482.
19 F. R. Fan, W. Tang and Z. L. Wang, *Adv. Mater.*, 2016, **28**, 4283.
20 X. J. Zhao, S. Y. Kuang, Z. L. Wang and G. Zhu, *ACS Nano*, 2018, **12**, 4280.
21 Y. C. Hu, H. J. Qiu, Q. J. Sun, Z. L. Wang and L. Xu, *Small Methods*, 2023, **7**, 2300582.
22 X. Li, J. Tao, X. Wang, J. Zhu, C. Pan and Z. L. Wang, *Adv. Energy Mater.*, 2018, **8**, 1800705.
23 X. Sun, C. J. Shang, H. X. Ma, C. Z. Li, L. Xue, Q. Y. Xu, Z. H. Wei, W. L. Li, Y. Yalikun, Y.-C. Lai and Y. Yang, *Nano Energy*, 2022, **100**, 107540.
24 S. Y. Wang, P. Xu, J. H. Liu, H. Wang, J. C. Si, J. Deng, M. Y. Xu and Z. L. Wang, *Nano Energy*, 2023, **118**, 109018.
25 Y. Wu, Y. Su, J. Bai, G. Zhu, X. Zhang, Z. Li, Y. Xiang and J. Shi, *J. Nanomater.*, 2016, **2016**, 1.
26 Q. Gao, Y. H. Xu, X. Yu, Z. X. Jing, T. H. Cheng and Z. L. Wang, *ACS Nano*, 2022, **16**, 6781.
27 C. C. Shan, W. C. He, H. Y. Wu, S. K. Fu, K. X. Li, A. P. Liu, Y. Du, J. Wang, Q. J. Mu, B. Y. Liu, Y. Xi and C. G. Hu, *Adv. Funct. Mater.*, 2023, **33**, 2305768.
28 S.-T. Chen, *J. Hydroinf.*, 2019, **21**, 343.
29 D. Yao, X. D. Liang, Q. Meng, J. Li, C. Wu, Z. S. Xie, D. D. Chen and J. P. Guo, *Sci. Bull.*, 2019, **64**, 143.
30 M.-J. Chang, H.-K. Chang, Y.-C. Chen, G.-F. Lin, P.-A. Chen, J.-S. Lai and Y.-C. Tan, *Water*, 2018, **10**, 1734.
31 H. J. Xiao and M. Y. Wei, *J. Coastal Res.*, 2018, **82**, 200.
32 W. C. Wang, J. C. Xu, H. W. Zheng, F. Q. Chen, K. Jenkins, Y. H. Wu, H. Y. Wang, W. F. Zhang and R. S. Yang, *Nanoscale*, 2018, **10**, 14747.
33 Q. F. Zheng, L. M. Fang, H. Q. Guo, K. F. Yang, Z. Y. Cai, M. A. B. Meador and S. Q. Gong, *Adv. Funct. Mater.*, 2018, **28**, 1706365.
34 W. C. Wang, J. W. Zhang, Y. J. Zhang, F. Q. Chen, H. Y. Wang, M. J. Wu, H. Li, Q. Y. Zhu, H. W. Zheng and R. Y. Zhang, *Appl. Phys. Lett.*, 2020, **116**, 023901.
35 Z. L. Wang, *Mater. Today*, 2017, **20**, 74.
36 S. M. Niu, Y. Liu, S. H. Wang, L. Lin, Y. S. Zhou, Y. F. Hu and Z. L. Wang, *Adv. Mater.*, 2013, **25**, 6184.
37 L. Chen, H. Y. Guo, X. N. Xia, G. L. Liu, H. F. Shi, M. J. Wang, Y. Xi and C. G. Hu, *ACS Appl. Mater. Interfaces*, 2015, **7**, 16450.
38 X. Wang, Z. Wen, H. Y. Guo, C. S. Wu, X. He, L. Lin, X. Cao and Z. L. Wang, *ACS Nano*, 2016, **10**, 11369.
39 X. X. Chen, H. Guo, H. X. Wu, H. T. Chen, Y. Song, Z. M. Su and H. X. Zhang, *Nano Energy*, 2018, **49**, 51.